International Journal of Geo-Information

MDPI

Article

Spatio-Temporal Coupling Between Urban Agglomeration Transport Networks and New Energy Vehicle Supply Chains: A GIS-Based Coupling-Coordination Analysis in the Pearl River Delta, China

Zhonghai Jiang [1,2] and Zhiyun Zou [1,*]

[1] School of Civil and Hydraulic Engineering, Huazhong University of Science and Technology, 1037 Luoyu Road, Wuhan 430074, China
[2] School of Civil Engineering and Transportation, Foshan University, 18 Jiangwan Road, Foshan 528000, China
* Correspondence: zyzou@hust.edu.cn

Abstract

Urban agglomeration transport networks and new energy vehicle (NEV) supply chains are spatially intertwined, yet the mechanisms governing their joint evolution remain insufficiently quantified from a geographic information science perspective. This study develops a dual-system coupling-coordination framework to examine this spatio-temporal coupling in the Pearl River Delta (PRD), China, one of the world's largest manufacturing regions and China's leading NEV production base. Using 62 functional spatial units, we compute comprehensive accessibility from a 62 × 62 multimodal travel time matrix generated by the OSRM routing engine on OpenStreetMap data (2025), and assign 12,986 verified supplier–buyer relationships among 8150 geocoded firms to three five-year windows (2011–2025). Effective inter-unit supply chain edges increased from seven to 131, while the supply chain Gini coefficient (0.611) far exceeded the accessibility Gini (0.161), revealing pronounced concentration along the Guangzhou–Shenzhen corridor. The coupling-coordination degree D ranged from 0.00 to 0.92 (mean = 0.43), and accessibility was positively associated with supply chain development (beta = 0.271, R2 = 0.068, $p = 0.041$). Scenario simulations indicate that supply chain resilience and innovation corridor investments are the most efficient per unit invested, whereas the comprehensive scenario yields the largest absolute gain in coupling coordination (delta D = +0.047). The study provides a transferable GIScience template for evidence-based transport-industry planning in large urban agglomerations.

Keywords: transport network; new energy vehicle; supply chain; urban agglomeration; coupling-coordination degree; accessibility; spatio-temporal analysis; geographic information science; OpenStreetMap; Pearl River Delta

Check for updates

Academic Editors: Wolfgang Kainz, Shivanand Balram, Eric Vaz and Suzana Dragicevic

Received: 11 September 2026
Revised: 19 November 2026
Accepted: 21 November 2026
Published: 26 November 2026

Copyright: © 2026 by the authors. Published by MDPI on behalf of the International Society for Photogrammetry and Remote Sensing. Licensee MDPI, Basel, Switzerland. This article is an open access article distributed under the terms and conditions of the Creative Commons Attribution (CC BY) license.

1. Introduction

1.1. Global Context: NEV Industrial Revolution and Supply Chain Spatial Organization

The electrification of personal transportation represents one of the most consequential industrial transitions of the twenty-first century. Global new energy vehicle (NEV) sales surpassed 14 million units in 2023, with China accounting for approximately 60 percent of the world market. This growth has been driven by a convergence of policy mandates (China's NEV Industry Development Plan 2021–2035 mandates 40 percent NEV penetration by 2030), declining battery costs, and rapidly expanding charging infrastructure [1]. Behind

these headline figures lies a spatially complex phenomenon: NEV supply chains are deeply disaggregated across multiple tiers of specialization, with battery cell manufacturing, electric drive systems, power electronics, and final assembly often performed by different firms distributed across city-regions hundreds of kilometers apart.

The spatial organization of NEV supply chains differs fundamentally from that of conventional automobiles. First, battery supply chains are globally extended: lithium, cobalt, and nickel inputs cross international borders, while cell production clusters in coastal China, South Korea, and Japan. Second, the electric drivetrain (motor, inverter, reducer, battery management system) requires just-in-time delivery from precision manufacturers concentrated in a small number of industrial districts. Third, charging infrastructure deployment depends critically on urban density and corridor traffic intensity, linking charging network planning to transport infrastructure investment [2]. These characteristics make NEV supply chains exceptionally sensitive to inter-urban transport conditions, and particularly vulnerable to accessibility bottlenecks in peripheral regions.

Urban agglomerations—the functional economic regions that contain integrated labor markets, specialized supplier networks, and shared infrastructure—provide the natural unit of analysis for studying NEV supply chain organization [3]. Batty formalizes cities as networks of networks [4], with transport infrastructure as the backbone that binds functional urban systems. Within an urban agglomeration, the co-location of assemblers, Tier-1 suppliers, and supporting services reduces logistics costs and facilitates knowledge spillovers, while intercity transport connections enable specialization across the broader region [5,6]. The quality of these connections—their speed, reliability, and coverage—shapes the effective economic distance between supply chain partners and, ultimately, the competitiveness of the regional industrial ecosystem [7].

1.2. Theoretical Foundations: Accessibility, Network Science, and Coupling Theory

Three bodies of theory inform this study. First, the accessibility literature, originating with Hansen [8] and extended by Geurs and van Wee [9], treats accessibility as the ease of reaching activities and opportunities through the transport system. This study adopts a min–max normalized travel time accessibility measure that captures the minimum multimodal travel time between each origin–destination pair, normalized to a 0–1 scale to ensure comparability across the 62 functional units.

Second, network science provides the analytical toolkit for representing and measuring supply chain structure. Following Borgatti and Foster [10], supply chain networks are represented as weighted undirected graphs in which nodes are spatial units and edges are verified supplier relationships. Key metrics include network density (the ratio of observed to possible edges), node degree (the number of distinct supply links), and weighted degree (the total volume of supply relationships). These metrics reveal not only the quantity but also the spatial pattern of supply chain integration [10,11].

Third, coupling-coordination theory, developed in the regional science and environmental economics literature [12] and applied to transport–industry coupling [13], treats the transport system and the supply chain system as interacting subsystems of a regional economy. The coupling degree C captures the intensity of interaction between the two systems; the coordination level T reflects their relative development; and the coupling-coordination degree D integrates both dimensions into a single metric. High D values indicate that both systems are well-developed and mutually supportive; low D values indicate imbalance or dysfunction in one or both systems [14].

1.3. Literature Review and Spatial–Analytical Research Gaps

Empirical research on transport–supply chain linkages falls into three streams. The first stream examines the effect of transport infrastructure on industrial location and productivity. Liu et al. [1] find that highway investment significantly raises manufacturing output per square kilometer in Chinese cities, with stronger effects in regions with pre-existing industrial clusters. Rocha et al. [6] document positive agglomeration effects from motorway network expansion in Portugal, with heterogeneous impacts across urban and peripheral locations.

The second stream investigates supply chain network structure and evolution. Wu et al. [13] find that highway transportation and new urbanization exhibit significant coupling coordination in Heilongjiang Province, with coupling degree increasing over time. Li et al. [12] apply the coupling-coordination model to transport and economic development in the Yangtze River Delta, finding that coupling coordination has improved since 2010 but remains spatially polarized [15].

The third stream analyzes supply chain resilience, particularly in the automotive sector. Raaymann and Spinler [16] systematically review supply chain resilience measurement in the automotive industry, finding that geographic concentration of supplier bases is a major vulnerability. Femano and Breitbach [2] develop evidence-based frameworks for measuring resilience strategy investments in supply chain networks. Yao et al. [17] demonstrate that transport network radiation effects significantly enhance industrial co-agglomeration within urban agglomerations. Despite this rich literature, three critical gaps remain: (1) most studies measure supply chain activity with aggregate proxies rather than explicit network data; (2) analyses are typically conducted at the city level, ignoring intra-city spatial heterogeneity; and (3) scenario simulations grounded in real infrastructure investment plans are rare, limiting policy relevance.

1.4. Research Objectives and Contributions

This study pursues four research objectives: (1) to quantify comprehensive transport accessibility at the functional-unit level (62 units) using a multimodal 62 × 62 travel time matrix; (2) to construct NEV supply chain networks from verified supplier–buyer relationships and trace their spatio-temporal evolution across three five-year windows; (3) to measure the coupling-coordination degree between the transport system and the supply chain system, including spatial autocorrelation analysis; and (4) to simulate alternative transport investment scenarios from the Guangdong 15th Five-Year Plan and evaluate their efficiency in improving coupling coordination.

The contributions are threefold. Methodologically, to our knowledge, this study is among the first to combine OSRM-derived travel time matrices, enterprise geocoding, and verified supply chain relationship data to construct fine-grained supply chain networks at the functional-unit scale in a Chinese urban agglomeration; prior city-level coupling studies relied on aggregate proxies [1,12]. Empirically, the study documents the dual-core (Guangzhou–Shenzhen) architecture of the PRD NEV supply chain and its rapid spatial deepening over 2011–2025. From a policy standpoint, the scenario simulations provide a quantitative basis for prioritizing near-term transport investments in supply chain-critical corridors.

1.5. Study Area: The Pearl River Delta Urban Agglomeration

The Pearl River Delta (PRD) is one of the world's most economically integrated urban agglomerations, comprising nine prefecture-level cities (Guangzhou, Shenzhen, Dongguan, Foshan, Zhongshan, Zhuhai, Huizhou, Jiangmen, and Zhaoqing) with a combined area of approximately 55,000 square kilometers and a population exceeding 80 million. Castells [18]

characterizes such large urban regions as the spatial form of the network society, in which flows of capital, information, and logistics organize economic activity across metropolitan boundaries. The PRD is China's largest manufacturing base and its leading NEV producing region, home to BYD (headquartered in Shenzhen), GAC Group (Guangzhou), and XPeng (Guangzhou/Shenzhen). The region's NEV output in 2024 exceeded 3 million units, approximately one-quarter of China's total NEV production.

The PRD's transport infrastructure has undergone rapid transformation over the study period. The Guangzhou–Shenzhen Expressway was augmented by the Guangzhou–Shenzhen Intercity Railway (opened 2011), the Shenzhen–Dongguan–Huizhou Intercity Railway (opened 2016), and the Foshan–Guangzhou–Zhuhai Intercity Railway (opened 2020). High-speed rail connections and the Shenzhen–Zhongshan Bridge corridor have further compressed intercity travel times [3]. These infrastructure developments provide variation in accessibility that is both spatially and temporally meaningful, making the PRD an ideal natural experiment for studying transport–supply chain coupling [19].

1.6. Contributions to Geo-Information Science

Beyond its substantive findings, this study offers three contributions to geographic information science and applied spatial analysis. First, it operationalises the functional spatial unit (FSU) as a fine-grained geographic unit of analysis for transport–supply chain coupling studies, replacing the conventional administrative-city boundary with units that better capture intra-metropolitan heterogeneity in commuting, land use, and industrial clustering; the delineation workflow is reproducible and can be transferred to other Chinese urban agglomerations or to metropolitan areas elsewhere. Second, it demonstrates how enterprise-level geocoding, combined with a multimodal OSRM travel time surface constructed from OpenStreetMap, can be used to reconstruct high-resolution supply chain networks that preserve relational structure while remaining computationally tractable; the resulting accessibility and supply chain surfaces are directly amenable to standard GIS operations (overlay, spatial join, rasterisation, and spatial autocorrelation). Third, by integrating coupling-coordination modeling, spatial regression, and counterfactual scenario analysis with the routing-engine accessibility surface, the framework provides a replicable GIScience template for evaluating regional transport investment plans in data-rich urban agglomerations, one that complements ex ante cost–benefit analysis with spatially explicit coupling diagnostics. Consistent with MDPI's data availability policy for *ISPRS International Journal of Geo-Information*, the geocoded firm coordinates, OSRM-derived travel time matrices, network statistics, and analysis scripts used in this study are made openly available to facilitate replication, sensitivity testing, and extension by the geo-information community.

2. Materials and Methods

2.1. Study Area and Functional Spatial Unit Delineation

A critical methodological choice is the spatial unit of analysis. City-level units mask substantial intra-city heterogeneity. To address this, this study adopts a functional-region delineation based on township-level administrative boundaries, resulting in 62 functional spatial units across the nine-city PRD region. This approach follows the functional urban area (FUA) methodology endorsed by the OECD and Eurostat [4] and applied to Chinese urban agglomerations by Liu et al. [20]. The 62 units are derived from the PRD township-level geographic base aggregated into functional clusters using employment density, road connectivity, and administrative contiguity criteria. Each unit is assigned a unique code (e.g., GZ01, SZ01, DG01) and attributed with city membership and zone type (core, transition, or periphery). Three rules made the aggregation reproducible. Townships whose employment density exceeded the regional median were treated as urbanized, a threshold taken from

the distribution of enterprise-registered employment rather than from an administrative classification. Contiguous urbanized townships joined by the OSM road network were then merged into a single cluster, and any cluster consisting of one detached township was attached to its administratively adjacent neighbor. The resulting units follow township boundaries, never cross prefecture-level city boundaries, and inherit the zone labels defined in Table 1 and Figure A1 map the resulting boundaries against the township base.

Table 1. Functional spatial units by city.

City (Code)	Units	NEV Industry Status	Zone Type
Guangzhou (GZ)	8	BYD (P Guangzhou), GAC, Xiaopeng	Core/Transition
Shenzhen (SZ)	7	BYD (HQ), Huawei, CATL R&D	Core
Dongguan (DG)	10	Oppo/Vivo supply chain, BYD plant	Core/Transition
Foshan (FS)	8	HEV cluster, parts supply	Core/Transition
Zhongshan (ZS)	5	Lighting/home appliances to NEV parts	Transition/Periphery
Zhuhai (ZH)	4	GEM, new energy equipment	Periphery
Huizhou (HZ)	7	BYD Blade Battery, TCL EV	Transition/Periphery
Jiangmen (JM)	7	CIMC, modern industry	Periphery
Zhaoqing (ZQ)	6	NEV industrial park	Periphery

Note: Zone type follows a three-tier classification: core (within 20 km of city center), transition (20–50 km), and periphery (>50 km). NEV industry status based on enterprise registration data.

Table 1 and Figure A1 reports the unit distribution by city. Guangzhou and Shenzhen have the highest number of units (8 and 7, respectively), reflecting their larger administrative areas and greater internal heterogeneity. The centroid coordinates of all 62 units serve as the origin points for the OSRM routing engine and as the matching targets for enterprise geocoding.

2.2. Transport Network Data and OSRM Routing

Transport network data were extracted from OpenStreetMap (OSM) vector files for three cross-sectional years: 2015, 2020, and 2025. The OSM data include all motorable road segments (motorway, trunk, primary, secondary, tertiary) and rail lines (high-speed rail, intercity rail, conventional rail) within the PRD boundary. The 2025 network layer contains 18,742 road segments and 47 rail segments, with a combined length of 24,381 km [8,9].

The OSRM routing engine was used to compute point-to-point travel times between all 62 unit centroids. For each origin–destination (OD) pair, OSRM returned the fastest route under a multimodal strategy. Road times came from the routing graph with speed profiles differentiated by road class (motorway: 100 km/h, trunk: 80 km/h, primary: 60 km/h, secondary: 40 km/h, tertiary: 30 km/h), with junction penalties handled internally by the engine. Rail times were computed along the OSM rail geometry between the stations nearest to each OD pair, with high-speed, intercity, and conventional services distinguished by their OSM maxspeed tags and a fixed dwell time of 3 min per intermediate stop. The shorter of the two times was taken as the effective travel time, on the assumption that travelers choose the faster mode. All times are free-flow estimates and therefore exclude congestion, a limitation taken up in Section 4.4. The resulting 62 × 62 travel time matrix (3782 OD pairs (62 × 62 matrix excluding the diagonal), 100% valid entries) provides the foundation for all accessibility calculations. Figure A2 presents the complete travel time matrix as a heatmap.

2.3. Enterprise Database and NEV Supply Chain Construction

NEV supply chain relationships were extracted from the Tianyancha enterprise database (tianyancha.com), China's most comprehensive commercial registration database. The query targeted NEV-related firms using a keyword dictionary covering six industrial

segments: (1) battery materials and manufacturing; (2) electric drive systems; (3) vehicle body and chassis; (4) charging infrastructure; (5) vehicle assembly; and (6) energy storage and power systems. This query returned 8150 unique NEV-related firms with valid registration addresses within the PRD boundary [21].

Each firm was geocoded by matching its registered address to the 62-unit framework via a two-step procedure: city/district name extraction by regular expression matching, followed by KD-tree nearest-neighbor matching of firm coordinates to unit centroids in EPSG:4490. This achieved an 88 percent geocoding coverage rate. Supply chain relationships were constructed from supplier–buyer disclosures filed under China's commercial credit reporting requirements. A relationship was included if: (1) at least one party is a verified NEV-related firm; (2) the relationship is documented with a contract value or explicit supply description; and (3) both parties are geocoded to valid PRD units. This yielded 12,986 verified NEV supply chain relationships, spanning 2008–2025. Two cleaning steps were applied to the raw records. Duplicate registration records were merged by unified social credit code, keeping the most recent valid address for each firm. Supplier–buyer links were then screened to remove group-internal transactions, in which both parties share the same ultimate parent, and intra-unit links, in which both parties fall within the same FSU; only inter-unit links entered the network. The rise in effective edges from 7 to 131 should be read in this light, since part of it reflects the widening coverage of the commercial credit database between 2011 and 2025 rather than network change alone. Section 4.4 returns to this caveat.

2.4. Temporal Windowing and Network Construction

Supply chain networks were constructed for three five-year windows to capture temporal dynamics: 2011–2015 (Phase I: Embodied Growth), 2016–2020 (Phase II: Rapid Expansion), and 2021–2025 (Phase III: Deep Integration). Within each window, relationships were aggregated to the unit level: for each pair of units (i, j), the undirected edge weight w_{ij} equals the total number of verified supply relationships flowing between them. Relationships with $w_{ij} \geq 1$ were retained as valid network edges. Table 2 reports the complete network statistics for all three windows. Each window was paired with the network snapshot closest to its end: 2015 for Phase I, 2020 for Phase II, and 2025 for Phase III. Accessibility and coupling coordination were therefore compared across three network–supply chain pairs rather than interpolated within windows.

Table 2. Supply chain network statistics by five-year window.

Window	Relationships	Effective Edges (E)	Density (d)	Phase
2011–2015	349	7	0.004	Embryonic
2016–2020	2547	59	0.031	Expansion
2021–2025	7881	131	0.069	Integration

Note: Relationships = total verified supplier–buyer pairs in the window. Effective Edges = unit pairs with at least one supply relationship. Density $d = 2E/[N(N-1)]$, $N = 62$.

2.5. Comprehensive Accessibility Measurement

The comprehensive accessibility A_i of unit i is derived from the minimum travel time $T_{i,min}$ to all other units, following the accessibility evaluation framework of Geurs and van Wee [9],

$$A_i = \frac{T_{max} - T_{i,min}}{T_{max} - T_{min}} \quad (1)$$

where T_{max} and T_{min} are the maximum and minimum values of $T_{i,min}$ across all 62 units. This polar-normalization scheme ensures that $A_i = 1$ for the unit with the shortest minimum

travel time, and $A_i = 0$ for the unit with the longest minimum travel time. The accessibility measure captures four components of the transport system: local road density, intercity highway connectivity, rail accessibility, and network topology [8,9].

2.6. Bivariate Coupling-Coordination Model

The coupling coordination between the transport system (accessibility A) and the supply chain system (development level S) is quantified using a bivariate coupling-coordination model [12]:

$$C_i = 2 \times \sqrt{\frac{A_i \times S_i}{(A_i + S_i)^2}} \quad (2)$$

C_i ranges from 0 to 1, with higher values indicating stronger coupling. The coordination level T_i reflects the absolute development state of the coupled system:

$$T_i = 0.5A_i + 0.5S_i \quad (3)$$

The coupling-coordination degree D_i integrates both coupling intensity and development level [14]:

$$D_i = \sqrt{C_i \times T_i} \quad (4)$$

D_i ranges from 0 (complete imbalance) to 1 (perfect coordination). Four qualitative grades are defined: Grade I (high coordination, 0.80–1.00), Grade II (moderate coordination, 0.60–0.80), Grade III (low coordination, 0.40–0.60), and Grade IV (imbalance, 0.00–0.40) [13]. The supply chain development level S_i is the min-max normalized total weighted degree of unit i in the 2021–2025 supply chain network, capturing both upstream (supplier) and downstream (customer) connectivity. Equations (1)–(4) specify the model in full. Accessibility and supply chain development are both min-max normalized to [0, 1] by Equation (1); C is the coupling coefficient of Equation (2); T = α·u + β·v is the coordination term of Equation (3), with equal weights α = β = 0.5 as is usual in bivariate coupling studies; and D = (C × T)^(1/2) is the coupling-coordination degree of Equation (4). The grade thresholds of 0.40, 0.60 and 0.80 follow the classification used in [13]. Units with A = S = 0 have no defined coupling coefficient; for the single such unit (ZQ07) C and D are both set to 0, which leaves the reported statistics unchanged. Section 3.8 reports how alternative weights or normalization schemes shift D.

2.7. Network Metrics and Spatial Inequality

Three complementary indicators characterize supply chain network structure and spatial inequality. Network density measures the completeness of inter-unit connections [10]:

$$d = \frac{2E}{N(N-1)} \quad (5)$$

where E is the number of effective edges and N = 62. Node-weighted degree k_i measures the total supply link volume of unit i: $k_i = \sum_j w_{ij}$. The Gini coefficient measures spatial inequality of a variable across units, computed from the Lorenz curve [22]:

$$G = \frac{\sum_i \sum_j |x_i - x_j|}{2n^2 \bar{x}} \quad (6)$$

where n = 62, x_i is the variable of interest (A, S, or D), and $\bar{x}$ is its mean. Figure A3 presents the Lorenz curves for A (Gini = 0.161), S (Gini = 0.611), and D (Gini = 0.355).

2.8. Spatial Autocorrelation Analysis

To assess whether D exhibits spatial clustering, we compute the global Moran I statistic using a row-standardized inverse-distance spatial weight matrix derived from the travel time matrix [11]:

$$I = \frac{\sum_{i=1}^{N}\sum_{j=1}^{N} w_{ij}(x-\overline{x})}{\sum_{i=1}^{N}(x-\overline{x})^2 \sum_{i=1}^{N}\sum_{j=1}^{N} w_{ij}} \quad (7)$$

Positive I values indicate positive spatial autocorrelation (high-D units tend to cluster near other high-D units); all three I values are statistically significant (permutation test, p 0.05, 999 permutations), confirming that spatial clustering is not attributable to random variation. Figure A4 presents the Moran scatter plots for A, S, and D.

2.9. Regression Analysis

To quantify the effect of transport accessibility on supply chain development, we estimate the OLS model [23],

$$S_i = \alpha + (\beta \times A_i) + \varepsilon_i \quad (8)$$

where α is the intercept, β is the accessibility coefficient of supply chain development, and ε_i is the error term. Robust standard errors are used throughout to guard against heteroskedasticity. Given the cross-sectional design (N = 62) and the observational nature of the data, β is read as an association rather than a causal or behavioral elasticity; Section 4.4 sets out the diagnostics and the spatial-econometric extension that a causal reading would require.

2.10. Scenario Simulation Framework

Six investment scenarios are derived from the Guangdong Province 15th Five-Year Plan (2026–2030) transport infrastructure project list. The simulation adopts a transparent reduced-form model. For each scenario s, the projected accessibility improvement $\Delta A_{i,s}$ of unit i is

$$\Delta A_{i,s} = \gamma_s \times Inv_s \times w_{i,s} \quad (9)$$

where Inv_s is the total investment (CNY billion), γ_s is a project-specific accessibility-investment conversion coefficient, and $w_{i,s}$ is the corridor allocation weight (1.0 for units within the target corridor, 0.3 for adjacent units, normalized to sum to 1.0 across all 62 units) [24]. The corridor definitions follow the spatial coverage of each scenario's project portfolio. The induced supply chain response is obtained from the accessibility coefficient estimated in Section 2.9:

The corridor allocation weights ($w_{i,s}$ = 1.0 for units within the target corridor, 0.3 for adjacent units, normalized to sum to 1.0 across all 62 units) are derived from the Guangdong Province 15th Five-Year Plan project locations and the expected catchment area of each intervention. This simplified specification is a hypothesis-driven scenario assumption, not a model-derived optimal allocation; Section 4.2 discusses the policy implications within this framing. The conversion coefficients γ_s were assigned by intervention type according to the expected travel time saving of each project portfolio on the 2025 network, with new intercity rail corridors receiving larger values than expressway upgrades. The model transfers the estimated accessibility–supply chain association linearly and therefore does not represent saturation or network bottlenecks. Scenario results are accordingly reported as diagnostics under stated assumptions rather than as forecasts or policy rankings; Section 3.8 reports the sensitivity analysis performed here, and Section 4.4 identifies what a full uncertainty treatment would still require.

$$\Delta S_{i,s} = \beta \times \Delta A_{i,s} \quad (10)$$

The projected $D_{i,s}$ is recomputed from the updated $A_{i,s}$ and $S_{i,s}$ using Equations (2)–(4). Marginal efficiency measures cost-effectiveness, $ME_s = \Delta\overline{D}_s/Inv_s$, where $\Delta\overline{D}_s$ is the regional

mean coupling-coordination improvement under scenario s [25]. All scenarios are evaluated within this common framework.

3. Results

3.1. Spatial Distribution of Comprehensive Accessibility

Figure 1 presents the spatial distribution of comprehensive accessibility across the 62 functional units. The accessibility surface exhibits a clear core–periphery gradient consistent with the hub-and-spoke structure of the PRD transport network. The highest accessibility values (A 0.80) are concentrated in the Guangzhou urban core (GZ01, GZ02), the Shenzhen urban core (SZ01, SZ02), and the Dongguan central corridor (DG01, DG02), where multiple highway and rail corridors intersect. These units have the shortest minimum travel times to all other units, typically under 90 min to any destination in the PRD.

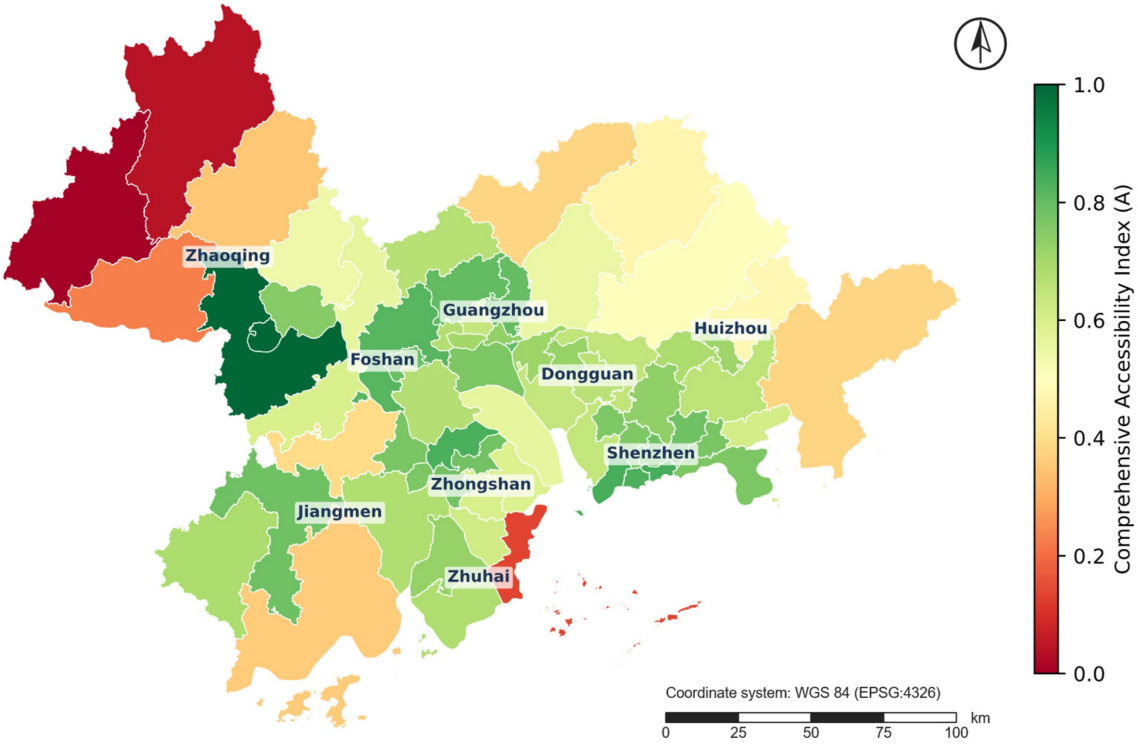

Figure 1. Spatial distribution of comprehensive accessibility (A) across 62 functional units in the Pearl River Delta (2025 network). Color scale: green = high accessibility (A = 0.80), yellow = moderate (0.50–0.80), red = low accessibility (A = 0.30). See Equation (1) for the accessibility formula. City abbreviations: GZ = Guangzhou, SZ = Shenzhen, DG = Dongguan, FS = Foshan, ZS = Zhongshan, ZH = Zhuhai, HZ = Huizhou, JM = Jiangmen, ZQ = Zhaoqing.

Moving outward from the core, accessibility declines steeply. Units in the Guangzhou–Huizhou border region (HZ01–HZ03) record A values in the 0.55–0.70 range, while the most peripheral Zhaoqing units (ZQ05, ZQ06) and western Jiangmen units (JM06, JM07) record A values below 0.25. The mean accessibility is 0.638 (SD = 0.199), and the accessibility Gini coefficient is 0.161, confirming the relatively even spatial distribution of transport provision across the 62 units. Table A2 reports the full accessibility rankings.

3.2. Spatial Pattern of NEV Supply Chain Activity

Figure 2 presents the NEV supply chain network for the 2021–2025 window, overlaid on the accessibility map. The supply chain network displays a striking core-concentration pattern: the top-10 hub units by weighted degree account for 52 percent of total network

activity, while the bottom-20 units account for less than four percent. The network is organized around two primary poles—the Guangzhou urban cluster (GZ01–GZ06, total weighted degree = 234) and the Shenzhen urban cluster (SZ01–SZ07, total weighted degree = 198)—consistent with the dual-core structure of the PRD economy.



Figure 2. Spatio-temporal evolution of NEV supply chain networks across three five-year windows: (**a**) 2011–2015 (E = 7, density = 0.004), (**b**) 2016–2020 (E = 59, density = 0.031), and (**c**) 2021–2025 (E = 131, density = 0.069). Arc thickness proportional to link weight; node size and color proportional to supply chain intensity S. See Table A1 for complete network statistics by window.

The supply chain Gini coefficient is 0.611, substantially higher than the accessibility Gini (0.161). This inequality gap—the 0.450-point difference—reveals that supply chain activity is far more spatially concentrated than transport provision. Figure A3 presents the Lorenz curves, confirming that the supply chain Lorenz curve is substantially below the accessibility Lorenz curve [26].

3.3. Spatio-Temporal Evolution of NEV Supply Chain Networks

The NEV supply chain network underwent three distinct phases of evolution between 2011 and 2025 (Figure 2). Phase I (2011–2015, the Embryonic Phase): only seven effective inter-unit edges were identified, corresponding to a network density of 0.004. At this stage, supply relationships were almost entirely confined within city boundaries. This pattern reflects the early-stage NEV market, in which production was concentrated in a few assembly plants with limited supplier network externalities.

Phase II (2016–2020, the Expansion Phase): The network expanded to 59 effective inter-unit edges (density = 0.031), an eight-fold increase in inter-unit connectivity. This expansion coincides with the rapid scale-up of NEV production following China's NEV subsidy policy expansion and the launch of Shenzhen's plate-based NEV purchase restrictions.

Phase III (2021–2025, the Integration Phase): The network reached 131 effective inter-unit edges (density = 0.069), with connections spanning all nine PRD cities. The opening of the Foshan–Guangzhou–Zhuhai Intercity Railway in 2020 and the Shenzhen–Zhongshan Bridge accelerated the westward integration of the supply chain. Figure A5 presents the A-S

coupling evolution diagram, showing the progressive rightward shift in the accessibility–supply chain distribution.

3.4. Coupling-Coordination Spatial Analysis

Figure 3 presents the spatial distribution of the coupling-coordination degree D. D ranges from 0.000 to 0.915 (mean = 0.434, SD = 0.277). High-coordination units (Grade I–II: D 0.60) are concentrated in the Guangzhou–Shenzhen–Dongguan corridor, where both accessibility and supply chain intensity are high. Low-coordination units (Grade IV: D 0.40) are found in peripheral Zhaoqing, western Jiangmen, and northern Huizhou.

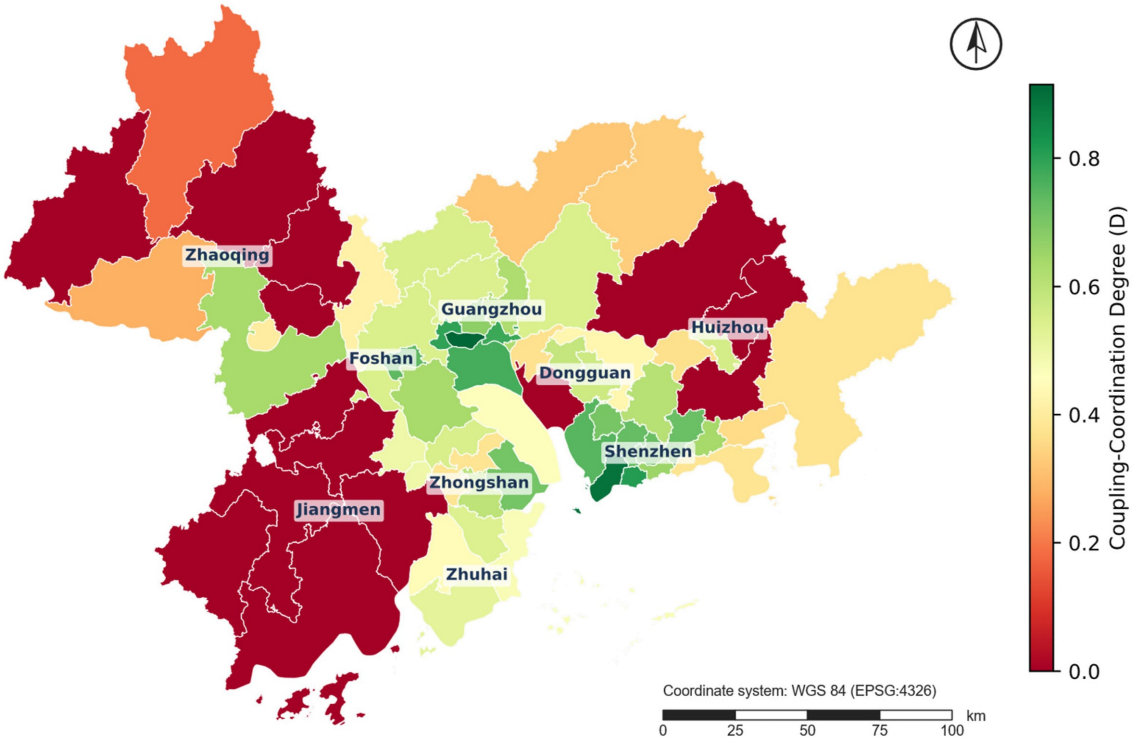

Figure 3. Spatial distribution of the coupling-coordination degree D between the transport system and the NEV supply chain system. See Equation (4) for the D formula. Grade I (D = 0.80–1.00, dark green): high coordination; Grade II (D = 0.60–0.80, light green): moderate coordination; Grade III (D = 0.40–0.60, yellow): low coordination; Grade IV (D = 0.00–0.40, red): imbalance [27].

The Moran I values (I_A = 0.030, I_S = 0.041, I_D = 0.047) confirm modest but positive spatial autocorrelation in all three key variables. These values suggest that spatial clustering is present but not dominant—high-D units are somewhat more likely to be near other high-D units, but the regional distribution is also shaped by unit-specific factors. Figure A4 presents the Moran scatter plots.

3.5. Regression Results: Association Between Accessibility and Supply Chain Development

Figure 4 and Table 3 report the OLS regression results. The estimated accessibility coefficient is β = 0.271* (R^2 = 0.068, p = 0.0413, N = 62). The positive and statistically significant coefficient indicates that higher transport accessibility is associated with higher supply chain development at the functional-unit level. Quantitatively, a 10-percentage-point improvement in normalized accessibility is associated with a 0.027-point improvement in normalized supply chain development. With a cross-sectional design and an R^2 of 0.068, this estimate is best read as an association. Spatial lag and spatial error models, additional socio-economic controls, and leverage diagnostics are left to future work (Section 4.4).

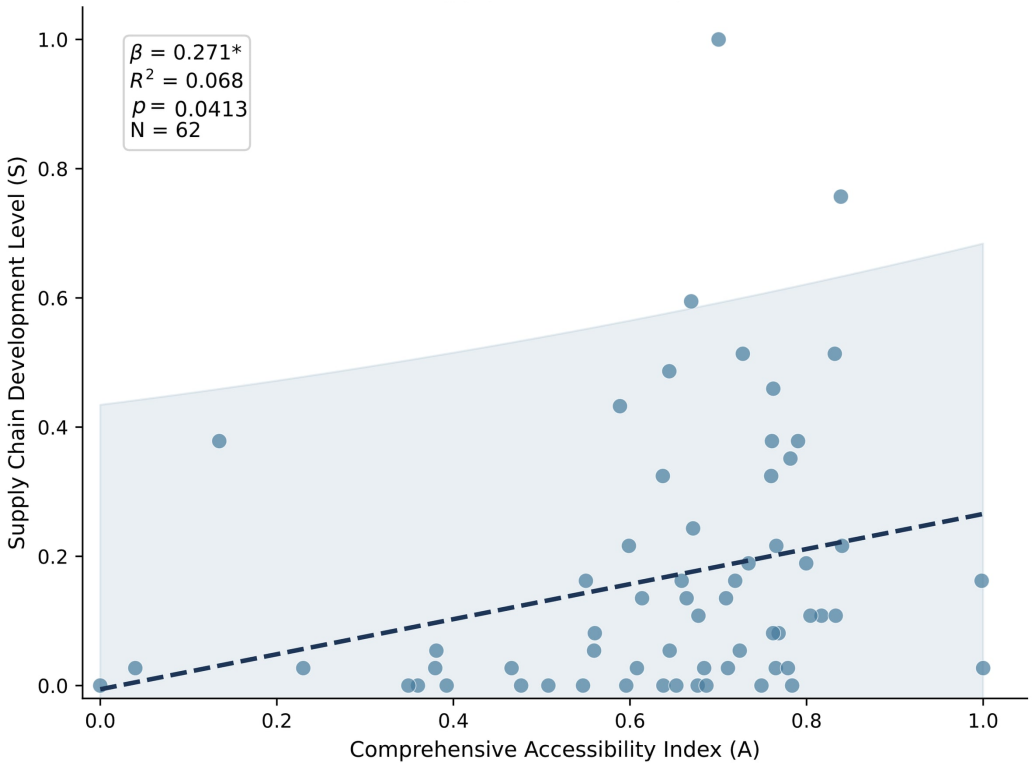

Figure 4. Impact of transport accessibility on NEV supply chain development. (Left) Scatter plot of supply chain development level (S) against comprehensive accessibility (A) for 62 units. Dashed line = OLS fit; shaded area = 95 percent CI. β = 0.271*, R^2 = 0.068, p = 0.0413, N = 62. See Equation (8) for model specification. (Right) Spatial distribution of regression residuals; red = above predicted, blue = below predicted. * denotes statistical significance at the 5% level ($p < 0.05$).

Table 3. OLS regression results: supply chain development (S) on comprehensive accessibility (A).

Variable	Coefficient	Std. Error	*t*-Value	*p*-Value	Significance
Intercept (alpha)	0.073	0.052	1.404	0.166	
Accessibility (A, beta)	0.271	0.130	2.085	0.041	*
R-squared	0.068				
Adj. R-squared	0.052				
Residual Std. Error	0.219	df = 60			
F-statistic	4.349	p = 0.041			*

Note: Robust standard errors in parentheses. * p = 0.05. See Equation (8).

The modest R^2 (0.068) indicates that transport accessibility explains only about seven percent of the variation in supply chain development across units. This finding is consistent with the view that supply chain development is shaped by multiple factors beyond transport accessibility: firm-specific capabilities, industrial policy, labor market conditions, land availability, and historical path dependencies all contribute to the observed spatial pattern [28].

3.6. Scenario Simulation Results

Table 4 and Figure 5 report the six investment scenarios and their outcomes. All scenarios improve regional mean coupling-coordination relative to the baseline ($\overline{D}$ = 0.434). S6 (comprehensive balance, CNY 1803 billion) achieves the largest absolute improvement, raising $\overline{D}$ from 0.434 to 0.481 (ΔD = +0.047, a 10.8 percent increase). S2 (transport priority, CNY 1200 billion) raises $\overline{D}$ to 0.470 (ΔD = +0.036). S4 (supply chain resilience, CNY 631

billion) and S5 (innovation corridor, CNY 637 billion) raise D to 0.466 (ΔD = +0.032) and 0.464 (ΔD = +0.030), respectively. These outcomes are model-based diagnostics under the assumptions set out in Section 2.10; they are neither forecasts nor a ranking of projects.

In terms of marginal efficiency (ME = ΔD/*Inv*), S4 (supply chain resilience, CNY 631 billion) ranks first with ME = 0.051 × 10^{-3} per CNY billion, marginally ahead of S5 (ME = 0.047 × 10^{-3} per CNY billion) and roughly twice the efficiency of S6 (ME = 0.026 × 10^{-3} per CNY billion). This finding indicates that investing in supply chain-critical links of the Sui–Guang–Shenzhen intercity rail corridor yields substantially higher coupling-coordination returns per unit of investment than broad network expansion. Here, Inv denotes the total investment in a scenario (CNY billion), as defined in Equation (9); it is not a logarithmic term.

S5 (innovation corridor, CNY 637 billion, ME = 0.047 × 10^{-3}/bn) and S3 (industry corridor, CNY 863 billion, ME = 0.038 × 10^{-3}/bn) follow in second and third place, and S2 (ME = 0.030 × 10^{-3}/bn) in fourth. S6 (ME = 0.026 × 10^{-3}/bn) is the least efficient per unit invested, reflecting diminishing marginal returns of very large investments spread across the entire network [29].

Table 4. Scenario simulation results: investment scale, coupling-coordination improvements, and marginal efficiency.

Scenario	Description	Investment (CNY bn)	$\overline{D}$ (After)	ΔD	ME (×10^{-3}/bn)	Rank
S1	Baseline (No Investment)	0	0.434	–	–	–
S2	Transport Priority (GZ-SZ)	1200	0.470	+0.036	0.030	4
S3	Industry Corridor (FS-GZ-DG-SZ)	863	0.466	+0.032	0.038	3
S4	Supply Chain Resilience (SZ-DG-HZ)	631	0.466	+0.032	0.051	1
S5	Innovation Corridor (GZ-ZS-ZH)	637	0.464	+0.030	0.047	2
S6	Comprehensive Balance (All)	1803	0.481	+0.047	0.026	5

Note: $\overline{D}$ = regional mean coupling-coordination degree. $\Delta\overline{D}$ = change in $\overline{D}$ relative to baseline. ME = $\Delta\overline{D}$/Inv, marginal efficiency in units of ×10^{-3} per CNY billion. CNY = Chinese Yuan.

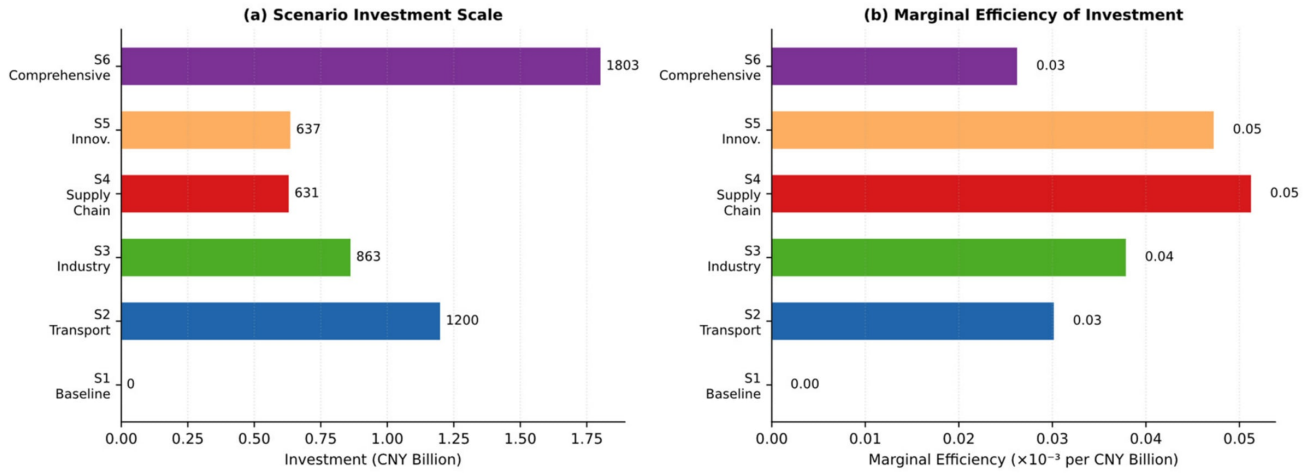

Figure 5. Scenario simulation of supply chain coupling improvement. (Left, panel **a**) Scenario investment scale (CNY billion) and resulting regional mean coupling-coordination $\overline{D}$. (Right, panel **b**) Marginal efficiency ME = $\Delta\overline{D}$/Inv (×10^{-3} per CNY billion). S4 achieves the highest ME (0.051, highlighted), marginally above S5 (0.047), indicating the largest coupling-coordination improvement per unit of investment. See Table 4 and Section 3.8 for full results.

3.7. A-S State Classification

Figure 6 presents the A-S state classification, revealing the four-quadrant structure of transport–supply chain coupling. The majority of peripheral units fall into Quadrant IV (Dual-Lagging), while the Guangzhou–Shenzhen core occupies Quadrant I (Synergetic). Figure A6 presents the top-20 rankings of functional units by each key indicator.

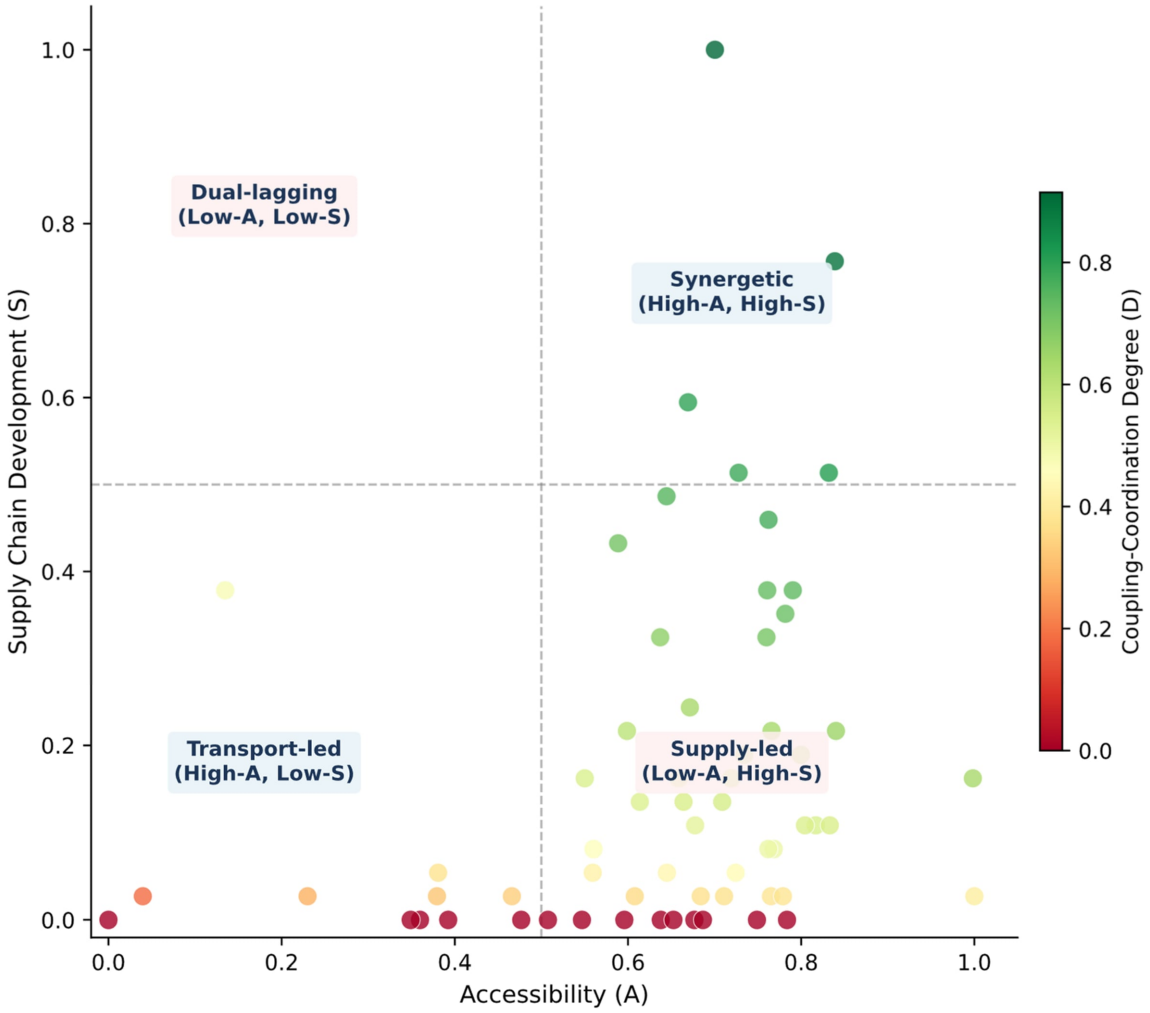

Figure 6. A-S state classification of 62 functional units into four quadrants: (I) Synergetic (high-A, high-S), (II) Transport-Led (high-A, low-S), (III) Supply-Led (low-A, high-S), and (IV) Dual-Lagging (low-A, low-S). Threshold lines at A = 0.5 and S = 0.5 define the quadrant boundaries. Point color represents the coupling-coordination degree D (Equation (4)).

3.8. Sensitivity Analysis

Two elements of the framework rest on judgment rather than estimation: the equal weighting of the coordination term and the conversion coefficients used in the scenarios. The weighting was re-examined by recomputing C, T and D for all 62 units with α set to 0.40, 0.45, 0.55 and 0.60 in turn (Table 5). The regional mean of D moves from 0.411 to 0.454 across this range, and the number of units in Grades I–II from 16 to 22, so the absolute grade counts should be read as indicative rather than fixed. The ordering of units is essentially unaffected: Spearman's ρ against the $\alpha = 0.5$ case is 0.999 or higher in every variant, and the Guangzhou–Shenzhen core and the peripheral cluster keep their positions. The substantive reading—a strongly concentrated core surrounded by weakly coupled peripheries—therefore does not depend on the choice of α.

Table 5. Sensitivity of the coupling-coordination results to the weighting of the coordination term.

α	Mean D	SD of D	Spearman ρ vs. α = 0.5	Units in Grades I–II
0.40	0.411	0.270	0.999	16
0.45	0.422	0.274	0.999	18
0.50	0.434	0.278	1.000	19
0.55	0.444	0.282	0.999	21
0.60	0.454	0.286	0.999	22

Note: C, T and D recomputed for all 62 units at each value of α, with $\beta = 1 - \alpha$. ρ is Spearman's rank correlation of unit-level D against the α = 0.5 baseline. Grade thresholds as defined in Section 2.6.

The scenario ranking is more sensitive to the conversion coefficients than to the coupling weights, because the marginal efficiency calculation is linear in both β and γ_s. Any uniform rescaling of β leaves every ME value proportional and the ranking unchanged, so the ordering in Table 4 does not depend on the precision of the regression estimate. What matters is the relative size of γ_s across scenarios. S4 remains the most efficient scenario unless its conversion coefficient is more than 8% below that used for S5, since the ratio of their ME values is 1.08; S5 stays ahead of S3 up to a 25% shortfall, and S3 ahead of S2 up to 26%. S4 and S5 should therefore be treated as equally efficient within the uncertainty attached to these assumptions, while both are clearly more efficient than S3, S2 and S6. This is the sense in which the scenario results are diagnostics: the ordering of the top two cannot be resolved without project-level travel time evidence.

4. Discussion

4.1. Theoretical Contributions

This study makes three theoretical contributions. First, by constructing supply chain networks from verified inter-firm relationships rather than aggregate output proxies, the study reveals the dual-core (Guangzhou–Shenzhen) architecture of the NEV supply chain and its rapid spatial deepening from seven to 131 effective inter-unit edges over 2011–2025. The finding that the supply chain Gini (0.611) is nearly four times the accessibility Gini (0.161) provides quantitative evidence that supply chain activity is far more spatially concentrated than transport provision [30].

Second, the bivariate coupling-coordination framework [31] treats transport and supply chain as two interacting systems, providing a transparent metric (D) that can be tracked over time and across space. The finding that D is bounded by the weaker system (supply chain) is consistent with coupling theory: at current levels of supply chain development, transport improvements alone generate limited D gains because the supply chain cannot absorb the induced demand.

Third, the Moran I analysis reveals modest but positive spatial autocorrelation in all three key variables ($I_A = 0.030$, $I_S = 0.041$, $I_D = 0.047$). These values, while modest, are consistent with the modest spatial clustering of NEV supply chain activity around the Guangzhou–Shenzhen core and adjacent Dongguan and Huizhou units—a pattern that resembles the centrifugal spatial diffusion process described in Krugman's New Economic Geography [32].

4.2. Policy Implications

Three policy implications follow from the findings. First, the high marginal efficiency of S4 (ME = 0.051×10^{-3} per CNY billion) suggests that under the assumed corridor weights, near-term investment should prioritize supply chain-critical links—the Sui–Guang–Shenzhen intercity rail, the Shenzhen–Dongguan intercity rail, and the Humen Bridge reconstruction—because these projects directly strengthen the corridors where sup-

ply chain density is highest [33]. The resulting supply chain response, amplified by the positive accessibility coefficient ($\beta = 0.271$), generates coupling-coordination improvements at roughly twice the rate of broad network expansion, though the modest R^2 (=0.068) indicates that this effect is limited in economic magnitude [32].

Second, the substantial share of Transport-Led units (high-A, low-S, approximately 11 units) indicates that further transport expansion alone will not equalize supply chain development. Complementary policies (supplier incubation programs, logistics hub development, NEV procurement platforms, and vocational training) are needed to convert improved accessibility into actual supply chain activity [16].

Third, the comprehensive scenario (S6) delivers the largest systemic improvement ($\Delta D = +0.047$) and is appropriate as a medium-term strategy once fiscal space allows. The aggregate coupling-coordination improvement is sufficient to elevate several currently low-coordination units into the moderate-coordination grade, with corresponding benefits for regional industrial cohesion [13]. Because the 62 FSUs are functional rather than administrative units, these recommendations need an implementation structure that matches them. Three levels suggest themselves. The provincial government, through the Development and Reform Commission and the Department of Transport, is the natural body for corridor investments that cross city boundaries, and the FSU diagnostics could feed into the five-year plan review. Municipal governments would deliver intra-city transport and land-use measures, using the FSU classification in Table 1 to sequence Transport-Led and Dual-Lagging units. A standing joint conference among the nine cities, building on existing PRD integration platforms, would align land supply, industrial policy and NEV procurement with corridor construction, so that complementary measures arrive alongside new capacity rather than after it.

4.3. Cross-Regional Comparison

The findings can be compared with those of related studies in other Chinese urban agglomerations. Li et al. [31] report a coupling-coordination mean of 0.412 between transport integration and economic development in the Yangtze River Delta (YRD) for the 2010–2020 period, lower than the PRD mean of 0.434, albeit with a broader definition of economic development. Wu et al. [23] report a transport–urbanization coupling-coordination of 0.381 in Heilongjiang Province, reflecting the lower transport integration of China's northeastern region. The PRD's supply chain Gini of 0.611 is comparable to the 0.55–0.65 range reported for automotive supply chain concentration in the Boston–Washington corridor [34], suggesting that the PRD's supply chain geography, while highly concentrated, is not atypical for large urban agglomerations in advanced economies.

4.4. Limitations and Future Research Directions

Five limitations should be noted. First, the supply chain network is built from firm registration and commercial credit records, which under-represent informal arrangements, intra-corporate transfers, and verbal agreements [21]. Second, accessibility is measured under free-flow conditions and therefore excludes congestion; time-dependent, peak-period routing would give a more realistic picture. Third, edge weights count verified relationships without regard to transaction volume or type, so a contract worth CNY 10 million and one worth CNY 10 billion enter the network identically. Fourth, the reduced-form scenario model assumes a linear accessibility–supply chain relationship and ignores saturation and bottlenecks [6,22]. Finally, the cross-sectional design identifies associations rather than causal effects: the OLS estimate in Section 3.5 is not a behavioral elasticity, and panel data with fixed effects, instrumental variables, or spatial lag and error specifications would be needed to go further [24].

5. Conclusions

This study examined the spatio-temporal coupling mechanism between urban agglomeration transport networks and NEV supply chains in the Pearl River Delta using a dual-system coupling-coordination framework. Five principal findings emerge from the analysis.

First, the NEV supply chain network evolved rapidly from seven to 131 effective inter-unit edges (density 0.004 to 0.069) across 2011–2025, organized around a persistent dual-core (Guangzhou–Shenzhen) spatial architecture. The supply chain Gini coefficient (0.611) is nearly four times the accessibility Gini (0.161), providing quantitative evidence that supply chain activity is far more spatially concentrated than transport provision.

Second, comprehensive accessibility exhibits a pronounced core–periphery gradient (mean = 0.638, SD = 0.199) consistent with the hub-and-spoke morphology of the PRD expressway network. The Moran I values ($I_A = 0.030$, $I_S = 0.041$, $I_D = 0.047$) confirm modest but positive spatial clustering in all three key variables.

Third, transport accessibility is positively and significantly associated with supply chain development in the baseline OLS model ($\beta = 0.271$*, $R^2 = 0.068$, $p = 0.0413$, N = 62). With a cross-sectional design, the estimate should not be read as a causal or behavioral elasticity. The modest R^2 also makes clear that accessibility is necessary but not sufficient: other factors shape supply chain outcomes.

Fourth, the coupling-coordination degree D ranges from 0.000 to 0.915 (mean = 0.434, SD = 0.277). High-coordination units (Grade I–II) are confined to the Guangzhou–Shenzhen–Dongguan core, while the majority of peripheral units fall into Grade IV (imbalance).

Fifth, scenario simulation shows that targeted supply chain resilience investment (S4: CNY 631 billion, primarily the Sui–Guang–Shenzhen intercity rail) achieves the highest marginal efficiency (0.051×10^{-3} per CNY billion), while the comprehensive scenario (S6: CNY 1803 billion) achieves the largest absolute coupling-coordination improvement ($\Delta D = +0.047$).

These findings support a sequenced policy strategy: (1) prioritize supply chain-critical corridor investments in the near term, particularly in the Shenzhen–Dongguan–Huizhou axis; (2) combine transport expansion with supply chain activation policies in Transport-Led units [32]; and (3) pursue comprehensive network upgrading as fiscal capacity allows, targeting the Dual-Lagging units in Zhaoqing, western Jiangmen, and northern Huizhou with integrated transport–industrial development programs.

Author Contributions: Zhonghai Jiang designed the study, analyzed data and wrote the manuscript. Zhonghai Jiang and Zhiyun Zou revised the manuscript. All authors have read and agreed to the published version of the manuscript.

Funding: The author received support from National Key RD Program of China (2022YFC3800103) for this study.

Data Availability Statement: The OSRM road network data are derived from OpenStreetMap (openly available at https://www.openstreetmap.org, accessed on 20 November 2026). Enterprise registration and supply chain relationship data were obtained from Tianyancha (https://www.tianyancha.com, accessed on 20 November 2026) under a commercial license and are not publicly available. The 62 × 62 travel time matrices, functional-unit boundary shapefiles, derived accessibility and supply chain indicators, and the analysis scripts (Python) are available from the corresponding author upon reasonable request.

Acknowledgments: The authors gratefully acknowledge the three anonymous reviewers and the academic editor for their constructive comments and careful handling of the manuscript, which substantially improved its quality. We also thank the editors and production team of *ISPRS International Journal of Geo-Information* for their professional support throughout the review and publication process.

Conflicts of Interest: The authors declare no conflicts of interest.

Appendix A

Table A1. Extended Supply Chain Network Statistics by Five-Year Window, with Hub Unit and Weighted Degree.

Window	Relationships	Effective Edges (E)	Density (d)	Top Hub Unit	Weighted Degree
2011–2015	349	7	0.004	GZ02	4
2016–2020	2547	59	0.031	GZ02	22
2021–2025	7881	131	0.069	GZ02	74

Table A2. Top-20 functional units by key indicators (2021–2025).

Rank	Unit	City	A (Accessibility)	S (Supply Chain)	D (Coupling Coordination)
1	GZ02	Guangzhou	0.700	1.000	0.915
2	SZ01	Shenzhen	0.839	0.757	0.893
3	SZ02	Shenzhen	0.832	0.514	0.808
4	GZ01	Guangzhou	0.669	0.595	0.794
5	GZ05	Guangzhou	0.728	0.514	0.782
6	GZ06	Guangzhou	0.762	0.459	0.769
7	SZ04	Shenzhen	0.645	0.486	0.748
8	FS01	Foshan	0.790	0.378	0.739
9	SZ06	Shenzhen	0.761	0.378	0.732
10	SZ05	Shenzhen	0.782	0.351	0.724
11	ZS02	Zhongshan	0.589	0.432	0.710
12	SZ07	Shenzhen	0.760	0.324	0.705
13	GZ03	Guangzhou	0.637	0.324	0.674
14	SZ03	Shenzhen	0.840	0.216	0.653
15	SZ08	Shenzhen	0.766	0.216	0.638
16	FS03	Foshan	0.671	0.243	0.636
17	ZQ03	Zhaoqing	0.998	0.162	0.634
18	GZ11	Guangzhou	0.800	0.189	0.624
19	DG03	Dongguan	0.734	0.189	0.610
20	ZS01	Zhongshan	0.599	0.216	0.600

Note: A = accessibility (min-max normalized, Equation (1)); S = supply chain intensity (min-max normalized weighted degree); D = coupling-coordination degree (Equation (4)).

Appendix B

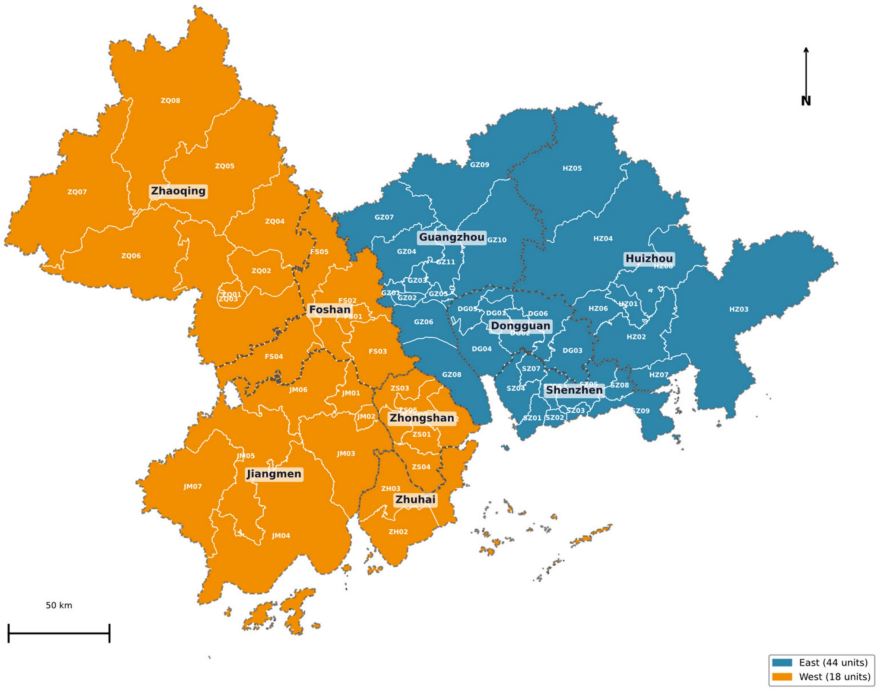

Figure A1. Spatial delineation of the 62 functional units in the Pearl River Delta. Numbers indicate unit codes (e.g., GZ01 = Guangzhou–Yuexiu, SZ01 = Shenzhen–Futian). Dashed lines denote city administrative boundaries; East-bank units are shaded blue and West-bank units orange, and unit centroids are marked by black dots.

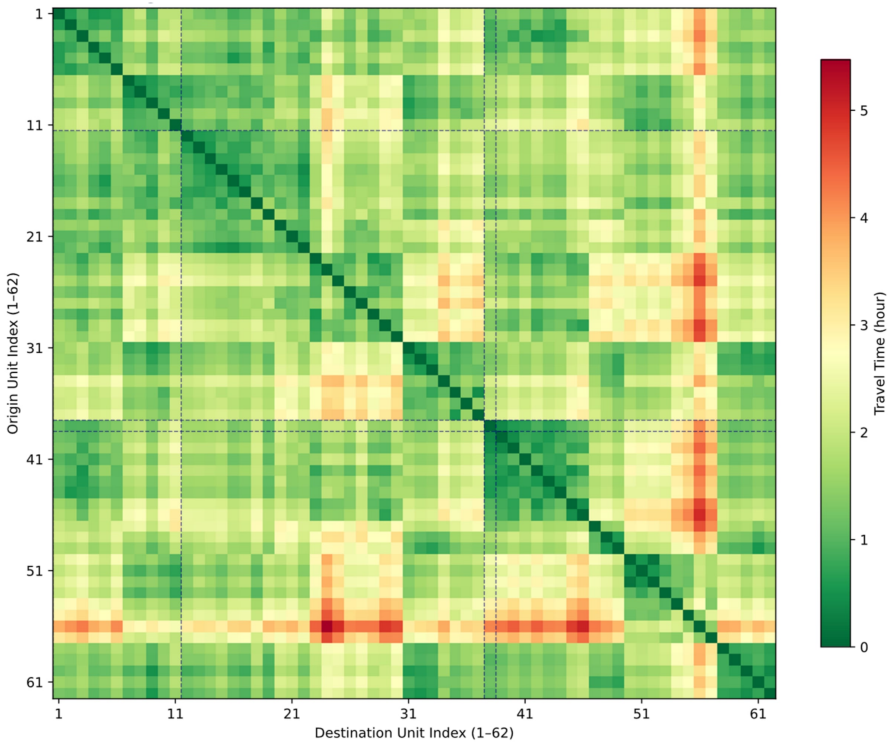

Figure A2. The 62 × 62 multimodal travel time matrix (hours) computed via OSRM on the 2025 road and rail network. Units ordered by city and accessibility rank. Color: green = short travel time (0.5 h), yellow = moderate (0.5–1.5 h), red = long travel time (2 h). Navy dashed lines mark the boundaries between major city clusters.

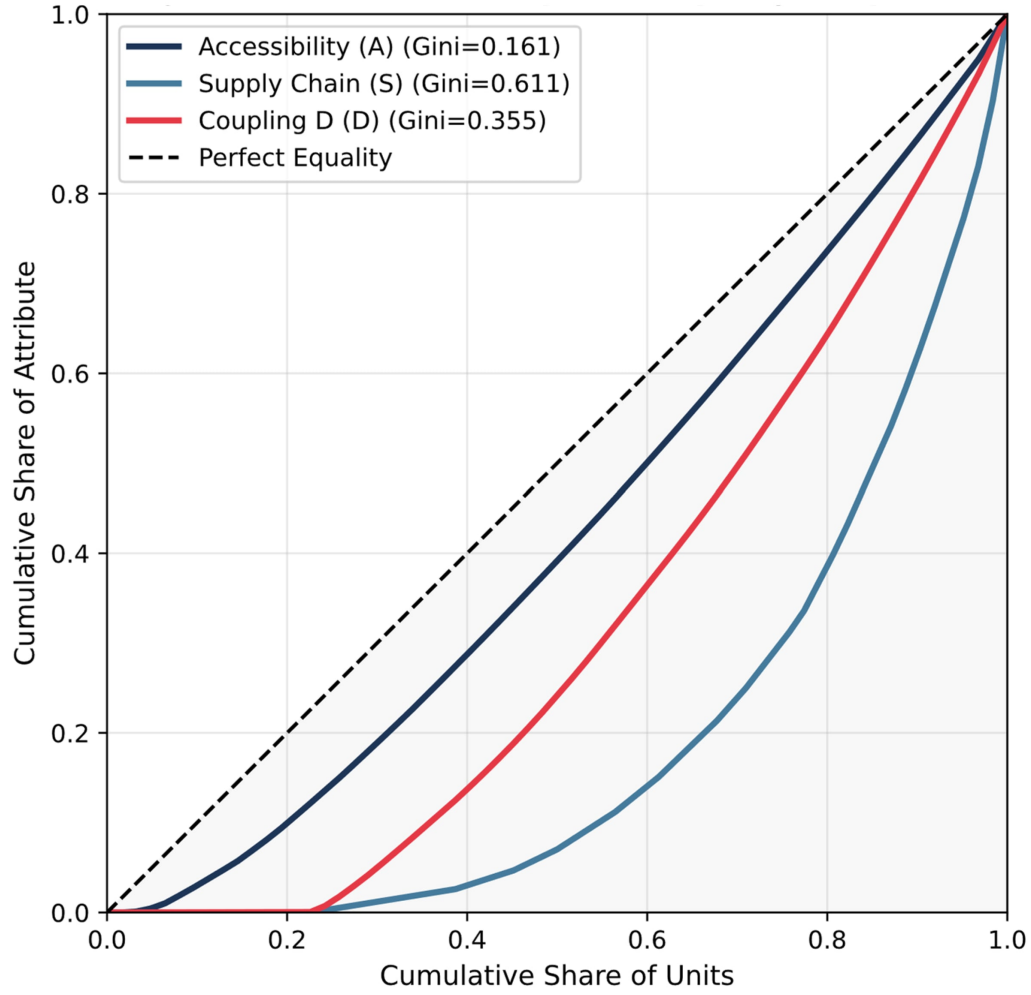

Figure A3. Lorenz curves for accessibility A (Gini = 0.161), supply chain S (Gini = 0.611), and coupling-coordination D (Gini = 0.355). See Equation (6) for the Gini formula.

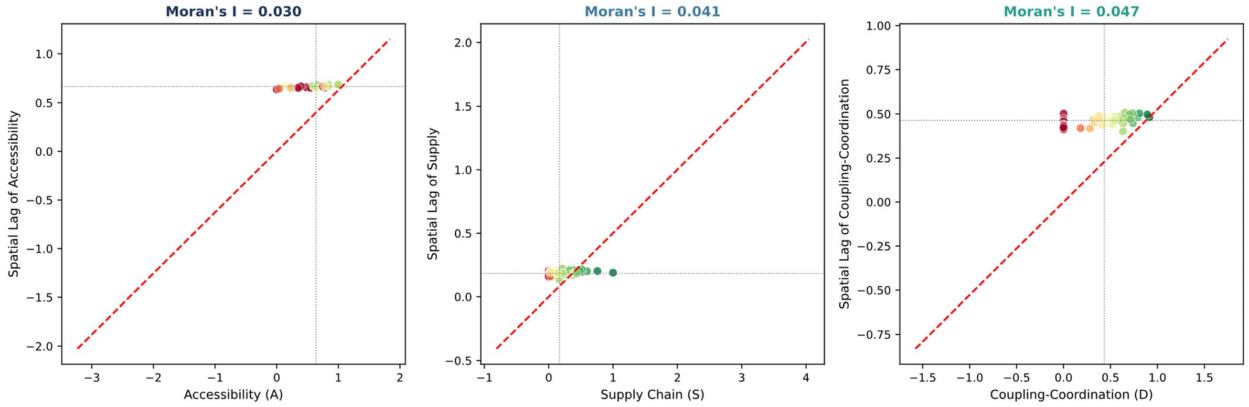

(**a**) (**b**) (**c**)

Figure A4. Moran scatter plots for (**a**) accessibility A (Moran's I = 0.030), (**b**) supply chain S (Moran's I = 0.041), and (**c**) coupling-coordination D (Moran's I = 0.047). See Equation (7) for Moran's I formula.

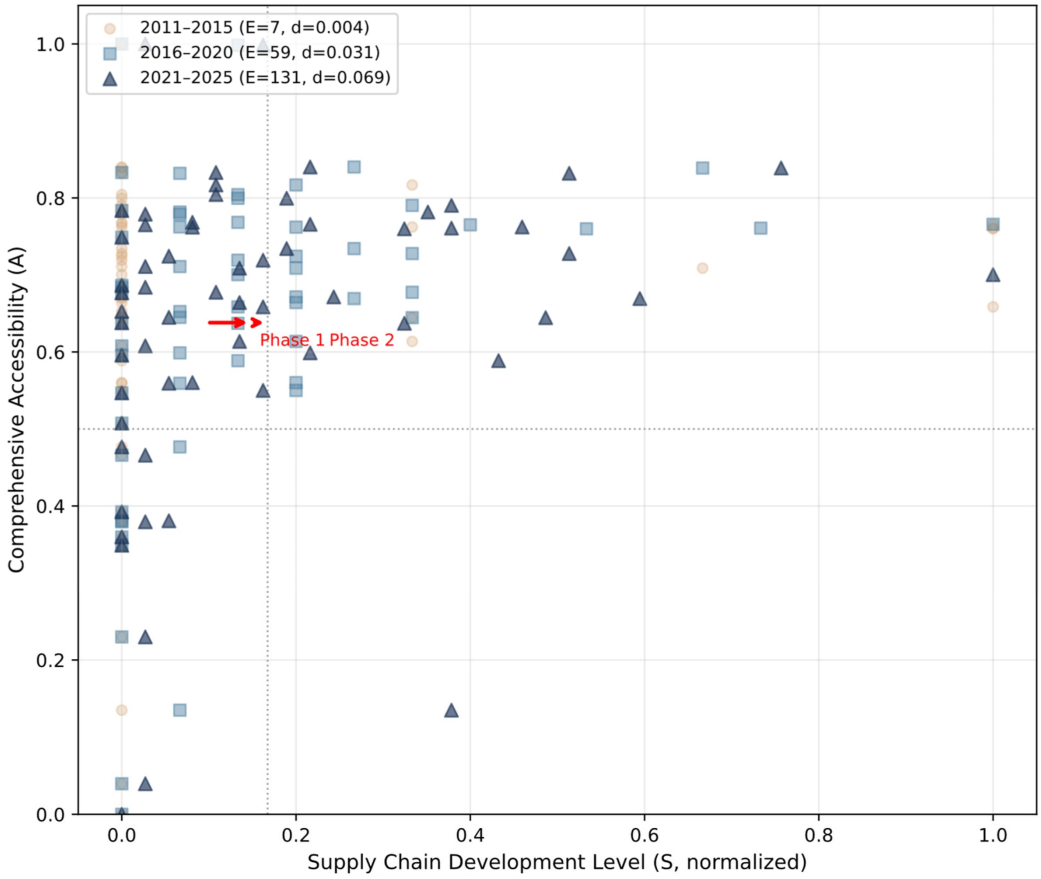

Figure A5. A-S coupling evolution across three five-year windows. Background scatter: unit positions in A-S space for each window (orange: 2011–2015, E = 7; blue: 2016–2020, E = 59; dark blue: 2021–2025, E = 131). Arrows show the trajectory of the regional mean S across windows.

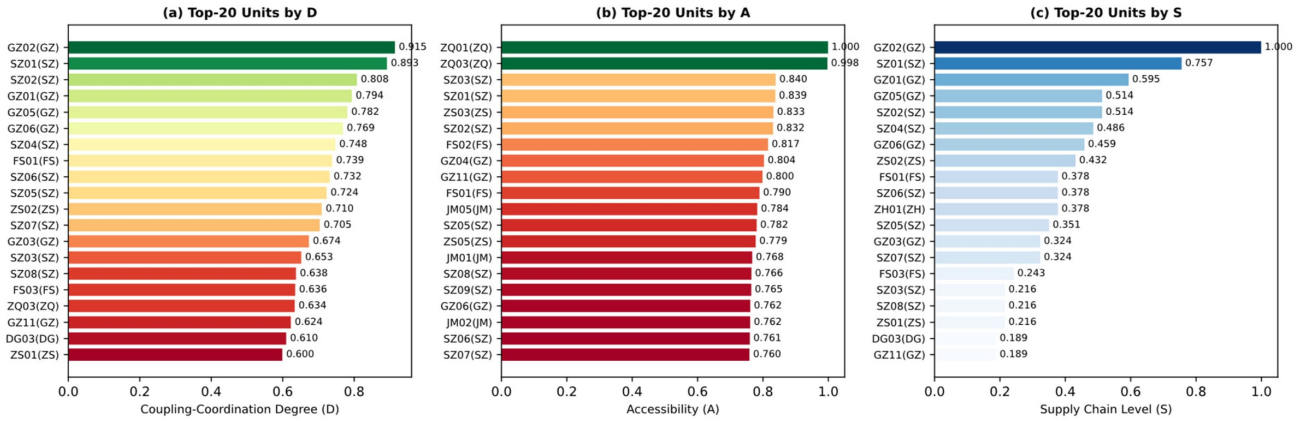

Figure A6. Top-20 functional units by (**a**) coupling-coordination degree D, (**b**) accessibility A, and (**c**) supply chain intensity S. GZ02 ranks first in both supply chain intensity (S) and coupling-coordination degree (D), whereas ZQ03 records the highest accessibility (A).

References

1. Liu, Z.; Zeng, J.; Jin, X.; Lu, T.; Ye, X. Transport infrastructure and industrial agglomeration: Evidence from manufacturing industries in China. *Transp. Policy* **2022**, *121*, 100–112. [CrossRef]
2. Femano, C.; Breitbach, N. Measuring supply chain resilience for informed resilience strategy investment. *Transp. J.* **2024**, *63*, e12037. [CrossRef]
3. Batten, D.F. Network cities: Creative urban agglomerations for the 21st century. *Urban Stud.* **1995**, *32*, 313–327. [CrossRef]
4. Batty, M. *The New Science of Cities*; MIT Press: Cambridge, MA, USA, 2013.

5. Krugman, P. Increasing returns and economic geography. *J. Polit. Econ.* **1991**, *99*, 483–499. [CrossRef] [PubMed]
6. Fujita, M.; Krugman, P.; Venables, A.J. *The Spatial Economy: Cities, Regions, and International Trade*; MIT Press: Cambridge, MA, USA, 1999; pp. 1–367.
7. Yu, Z.; Xiao, Z.; Liu, X. Characterizing the spatial-functional network of regional industrial agglomerations: A data-driven case study in China's greater bay area. *Appl. Geogr.* **2023**, *152*, 102901. [CrossRef]
8. Hansen, W.G. How accessibility shapes land use. *J. Am. Inst. Plan.* **1959**, *25*, 73–76. [CrossRef]
9. Geurs, K.T.; van Wee, B. Accessibility evaluation of land-use and transport strategies: Review and research directions. *J. Transp. Geogr.* **2004**, *12*, 127–140. [CrossRef]
10. Borgatti, S.P.; Foster, P.C. The network paradigm in organizational research: A review and typology. *J. Manag.* **2003**, *29*, 991–1013. [CrossRef]
11. Anselin, L. *Spatial Econometrics: Methods and Models*; Kluwer Academic Publishers: Dordrecht, The Netherlands, 1988.
12. Rocha, B.T.; Melo, P.C.; Afonso, N.; de Abreu e Silva, J. The local impacts of building a large motorway network on population and employment: Evidence from Portugal. *Econ. Transp.* **2023**, *34*, 100302.
13. Rivera-Gonzalez, C.; Holguin-Veras, J.; Calderon, O. Supply-chain-focused measures of centrality and spread in metropolitan areas. *J. Transp. Geogr.* **2023**, *107*, 103553. [CrossRef]
14. Yang, X.; Lu, S.; Chen, J.; Ye, X.; Liu, Z. Factor mobility, transportation network and green economic growth of the urban agglomeration. *Sci. Rep.* **2022**, *12*, 20038. [CrossRef] [PubMed]
15. Christopher, M.; Peck, H. Building the resilient supply chain. *Int. J. Logist. Manag.* **2004**, *15*, 1–14. [CrossRef]
16. Chopra, S.; Meindl, P. *Supply Chain Management: Strategy, Planning, and Operation*, 7th ed.; Pearson: London, UK, 2019; pp. 1–512.
17. Castells, M. *The Rise of the Network Society*; Blackwell Publishers: Oxford, UK, 1996; Volume I, pp. 1–597.
18. Yao, Y.; Ye, X.; Xiao, W.; Chen, J. Radiation effect of urban agglomeration transportation network: Evidence from Chengdu. *Land* **2021**, *10*, 520. [CrossRef]
19. Chen, J.W.; Luo, X.; Yeung, R.C. From World Factory to Global City-Region: The Dynamics of Manufacturing in the Pearl River Delta and Its Spatial Pattern in the 21st Century. *Land* **2024**, *11*, 625.
20. Liu, L.; Luo, X.; Rijal, S.; Zeng, J.; Jin, X. Spatial spillover effects of urban agglomeration on road network with industrial co-agglomeration. *Land* **2024**, *13*, 2097. [CrossRef]
21. Gu, M.; Yang, L.; Huo, B. The impact of information technology usage on supply chain resilience and performance: An ambidexterous view. *Int. J. Prod. Econ.* **2021**, *232*, 107956. [CrossRef] [PubMed]
22. Lorenz, M.O. Methods of Measuring the Concentration of Wealth. *Publ. Am. Stat. Assoc.* **1905**, *9*, 209–219.
23. Wu, B.; Jin, X.; Li, D.; Wang, B. Spatial-temporal evolution of coupling coordination development between regional highway transportation and new urbanization: A case study of Heilongjiang, China. *Sustainability* **2023**, *15*, 16365. [CrossRef]
24. LeSage, J.P.; Pace, R.K. *Introduction to Spatial Econometrics*; Chapman and Hall/CRC: Boca Raton, FL, USA, 2009.
25. Chen, D.; Wang, G.; Yuan, Z.; Zhang, E. Study on the Spatial Pattern and Influencing Factors of China's New Energy Vehicle Industry—Based on Data of Relevant Listed Companies from 2008–2021. *Sustainability* **2023**, *15*, 3058. [CrossRef]
26. Fiksel, J. Sustainability and Resilience: Toward a Systems Approach. *Sustain. Sci. Pract. Policy* **2006**, *2*, 14–21. [CrossRef]
27. Ponomarov, J.S.; Holcomb, M.C. Understanding supply chain resilience taxonomy. *Int. J. Logist. Manag.* **2009**, *20*, 476–498. [CrossRef]
28. Sheffi, Y.; Rice, J.B. A supply chain view of the resilient enterprise. *MIT Sloan Manag. Rev.* **2005**, *47*, 41–48.
29. Huo, B.; Li, D.; Gu, M. The impact of information sharing on supply chain learning and flexibility performance. *Int. J. Prod. Res.* **2020**, *59*, 1411–1434. [CrossRef]
30. Huang, X.; Guo, R.; Wang, W.; Li, X.; Fan, Y. Research on the Spatial Disparities and Convergence of Guangdong's Urban Economy Based on Industrial Agglomeration and Industrial Proximity. *Land* **2024**, *13*, 73. [CrossRef]
31. Li, S.; Song, Y.; Xia, W.; Fu, S. Regional Transportation Integration and High-Quality Economic Development, Coupling Coordination Analysis, in the Yangtze River Delta, China. *Systems* **2023**, *11*, 279. [CrossRef]
32. Raaymann, L.; Spinler, S. Measuring supply chain resilience along the automotive value chain—A comparative research on light-duty vehicles. *Transp. Res. Part E* **2024**, *190*, 103792.
33. Xu, Z.; Chopra, S.S. Interconnectedness enhances network resilience of multimodal public transportation systems for Safe-to-Fail urban mobility. *Nat. Commun.* **2023**, *14*, 4291. [CrossRef] [PubMed]
34. Ducruet, C.; Igarashi, Y. Ports and maritime networks. In *International Encyclopedia of Geography*; Wiley: Hoboken, NJ, USA, 2017; pp. 1–15.

Disclaimer/Publisher's Note: The statements, opinions and data contained in all publications are solely those of the individual author(s) and contributor(s) and not of MDPI and/or the editor(s). MDPI and/or the editor(s) disclaim responsibility for any injury to people or property resulting from any ideas, methods, instructions or products referred to in the content.